View Article Online / Journal Homepage / Table of Contents for this issue
Dynamic Article Links

Lab on a Chip

Cite this: *Lab Chip*, 2012, **12**, 546

www.rsc.org/loc

TUTORIAL REVIEW

Spintronic platforms for biomedical applications

P. P. Freitas,[ab] F. A. Cardoso,[a] V. C. Martins,*[ab] S. A. M. Martins,[ac] J. Loureiro,[a] J. Amaral,[a] R. C. Chaves,[a] S. Cardoso,[a] L. P. Fonseca,[c] A. M. Sebastião,[d] M. Pannetier-Lecoeur[e] and C. Fermon[e]

Received 22nd August 2011, Accepted 11th November 2011
DOI: 10.1039/c1lc20791a

Published on 07 December 2011. Downloaded by Universidade de Lisboa on 23/05/2017 15:50:11.

Since the fundamental discovery of the giant magnetoresistance many spintronic devices have been developed and implemented in our daily life (*e.g.* information storage and automotive industry). Lately, advances in the sensors technology (higher sensitivity, smaller size) have potentiated other applications, namely in the biological area, leading to the emergence of novel biomedical platforms. In particular the investigation of spintronics and its application to the development of magnetoresistive (MR) biomolecular and biomedical platforms are giving rise to a new class of biomedical diagnostic devices, suitable for bench top bioassays as well as point-of-care and point-of-use devices. Herein, integrated spintronic biochip platforms for diagnostic and cytometric applications, hybrid systems incorporating magnetoresistive sensors applied to neuroelectronic studies and biomedical imaging, namely magneto-encephalography and magneto-cardiography, are reviewed. Also lab-on-a-chip MR-based platforms to perform biological studies at the single molecule level are discussed. Overall the potential and main characteristics of such MR-based biomedical devices, comparing to the existing technologies while giving particular examples of targeted applications, are addressed.

1. Introduction

Increasing research in nanotechnology and its application to biomedical studies is leading to the development of more sensitive, faster, smaller and more user friendly equipment. In particular the investigation of spintronics and its application to the development of magnetoresistive (MR) biomolecular and biomedical platforms is giving rise to a new class of point-of-care and point-of-use devices.[1–3] In such devices the sensing elements are MR sensors, which presently find their major application in the data storage market, as read heads in hard disk drives (Fig. 1). Due to the advantage of being compatible with silicon integrated circuit fabrication technology, compact chips comprising single or multiple sensors along with the required electrical circuitry have been produced.

The electrical resistance of a MR sensor varies with an applied external magnetic field (Fig. 1). This variation is nearly linear in a relatively short magnetic field range (*i.e.* 50 Oe range), conferring quantitative sensing capacity.

Spin valves (SV) are a particular type of MR sensors composed of two ferromagnetic layers, one with a fixed magnetization and the other free to rotate with an external magnetic field, separated by a non-magnetic metal spacer. The angle between the magnetization directions dictates the resistance of the sensor. When they are in a parallel configuration the resistance is minimal while an antiparallel configuration produces a maximal resistance. Presently, SV sensors show magnetoresistance in the order of 7 to

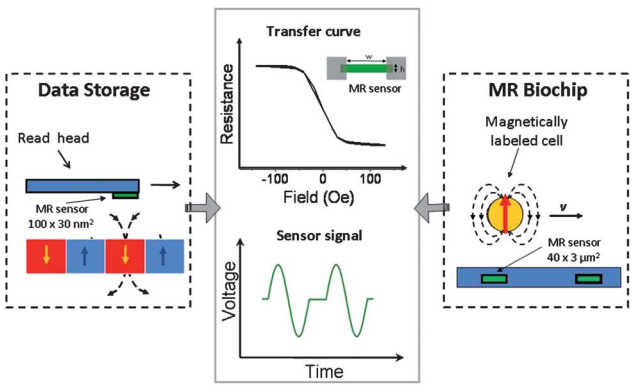

Fig. 1 MR sensors applied to data storage technology, particularly in read-heads, and to MR-based biochips, particularly in the detection of magnetically labeled cells. Typical transfer curve and electrical signals obtained in these two applications are shown.

[a]*INESC-MN—Instituto de Engenharia de Sistemas e Computadores-Microsistemas e Nanotecnologias and IN-Institute of Nanoscience and Nanotechnology, Rua Alves Redol, 9, 1000-029 Lisbon, Portugal. E-mail: veronica.romao@inl.int*
[b]*INL—International Iberian Nanotechnology Laboratory, Av. Mestre José Veiga, 4715-31 Braga, Portugal*
[c]*IBB—Institute for Biotechnology and Bioengineering, Center for Biological and Chemical Engineering (CEBQ), Instituto Superior Técnico, Av. Rovisco Pais, 1049-001 Lisbon, Portugal*
[d]*Institute of Pharmacology and Neurosciences, Faculty of Medicine and Institute for Molecular Medicine, University of Lisbon, Av. Prof. Egas Moniz, 1649-028 Lisbon, Portugal*
[e]*DSM/IRAMIS/SPEC—CNRS URA 2464, CEA Saclay, 91191 Gif-sur-Yvette, France*

This journal is © The Royal Society of Chemistry 2012

View Article Online

Published on 07 December 2011. Downloaded by Universidade de Lisboa on 23/05/2017 15:50:11.

15% under an applied field not higher than a few tens of Oe, leading to sensitivities around 0.1%/Oe.[3]

Therefore, due to their high sensitivity to magnetic fields, SV are now the most frequently used type of MR sensors applied to the detection of biological events in different biomedical devices. In fact, theoretical modeling confirmed by experimental results shows that highly sensitive MR sensors allow the detection of small magnetic fields enabling their usage in applications such as: measurement of biological signals coming from living organs (*e.g.* heart and brain);[4,5] discrimination of magnetic entities (*e.g.* magnetic-labeled cells) flowing at high speed;[6] detection of nanometre-sized magnetic particles used as biological labels;[7–9] or sensing nanometric displacements of magnetically labeled biomolecules.[10]

This paper will cover some of those applications, namely biochip platforms for biomolecular recognition detection,[11–14] lab-on-a-chip platforms for cell sorting and counting,[15] single molecule actuation and detection platforms[10] and hybrid platforms targeted at biomedical imaging.[4] A review on the state-of-the-art advances made by different groups in the various MR-based biomedical areas and a summary of the recent achievements attained at INESC-MN are presented.

Applications for the detection of DNA hybridization events (DNA-chips) are discussed. A particular example for flow cytometry (extraction and counting) of CD34+ magnetically labeled cells coming from bone marrow or cord blood samples is given. For single biomolecule studies on-chip magnetic tweezers were integrated with magnetoresistive sensors producing forces up to 1.0 ± 0.3 pN capable of magnetic bead actuation. The system developed is sensitive to the vertical displacement of a magnetic bead tagged DNA, caused by the activity of a molecular motor, with a resolution of 60 nm. Furthermore, for biomedical imaging applications, field sensitivity is being pushed below 1 pT $Hz^{-1/2}$ in hybrid devices incorporating flux guides with the magnetoresistive element allowing the direct detection of bio-magnetic fields from brain and heart. A system capable of performing and comparing electrical and magnetic measurements of a stimulated rat brain slice is also presented.

2. Diagnostic platforms

A new generation of biomedical diagnostic devices is needed for point-of-care applications. The availability of such devices will lead to more efficient disease prevention and improvement of patient quality of life, allowing for life-threatening events to be detected and controlled long before a critical stage is reached.

Therefore novel biomedical diagnostic devices with superior characteristics, namely high sensitivity, accuracy, specificity, reproducibility and response speed, automation of sample acquisition, processing, molecular detection and data analysis, miniaturization and autonomy envisioning portability and simple operation, are still required.

Biochip-based devices hold great potential to address all these requirements and are outstanding candidates to fulfil the market needs.[18]

More recently, a novel biochip detection system based on MR sensors associated with the use of superparamagnetic micro- and nano-particles as a reporter system has emerged with many promising characteristics.[12,13,16,19,20] High sensitivity, low background, tuneable dynamic range, fast performance and electronic platform compatibility leading to integrability, miniaturization, scalability, portability and low production costs are combined to originate valuable biomedical diagnostic tools.[21–24]

In a standard MR biochip-based bioassay, a recognition probe immobilized over the sensor is used to interrogate an unknown sample potentially containing a target molecule of interest (*e.g.* DNA strand, protein or cell antigens), labeled with a magnetic particle. Whenever there is recognition between the target and its probe, a biomolecular event occurs. After washing, the recognized targets stay over the sensor while the unbound molecules are washed out. Applying an external magnetic field, the magnetic labels attached to the bound molecules will create a fringe field further detected by the MR sensor (Fig. 2).

MR sensors allow a discrete quantification of magnetic entities which, when related to the number of molecular recognition events, results in a quantitative analytical mode, overcoming the "yes or no" basic type of answer presented by many technologies.

Moreover, magnetic particles, when associated with the target molecule, offer a number of advantages, such as: (i) target concentration from the native sample into a smaller volume of a different buffer solution, (ii) on-chip active transportation and (iii) site-focusing of the magnetically labeled molecules.[14] A relevant aspect is the fact that biological samples do not present "in nature" magnetic properties, circumventing the common problem of signal interference and background noise usually associated with other reporter systems (*e.g.* fluorescence, electrochemistry or enzymatic colorimetry).

Additionally, the combination of these MR biochips to electronic[1] and microfluidic platforms[25] may enable sample position control, temperature control, detection signal acquisition and processing, converting a bulky and complex analytical apparatus into a practical lab-on-a-chip device.[26]

Presently two main types of MR biochip platforms, in terms of biomolecular recognition agent in use, have been developed and applied to biomedical diagnostic; these are DNA-chips and immuno-chips, which use either DNA sequences or antibodies as biological probes immobilized over each sensing area, respectively.

In the literature, MR biochips have been used mostly as immuno-chips[27–32] rather than DNA-chips.[13,14,33]

The INESC-MN group has a DNA-chip at an advanced state of development where the detection of DNA hybridization signals has been optimized for biotinylated ssDNA, 20mer

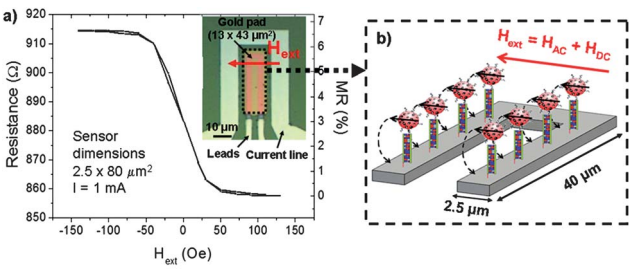

Fig. 2 Characteristics of a U-shaped spin-valve sensor. (a) Transfer curve and microscopic picture of the sensing site in the inset. (b) Schematic representation of the measurement conditions on a spin valve detecting magnetically labeled hybridized target DNA.

View Article Online

Published on 07 December 2011. Downloaded by Universidade de Lisboa on 23/05/2017 15:50:11.

sequence corresponding to the 16S ribosomal region of *E. coli*.[1,14] In parallel, on-going work on an immuno-chip is focusing on the detection of *Salmonella Thyphimurium* cells.[34]

The biochip comprises 28 bioactive sensors plus 4 reference sensors. The 2.5 × 80 μm² U-shaped spin-valve sensors were optimized in order to achieve a linear response as shown in Fig. 2a. An U-shaped current line surrounding the sensors was designed to enable particles focusing onto the sensing area.[35]

The sensor stack is typically: 20 Å Ta/30 Å $Ni_{80}Fe_{20}$/25 Å $Co_{81}Fe_{19}$/26 Å Cu/25 Å $Co_{81}Fe_{19}$/60 Å $Mn_{76}Ir_{24}$/30 Å Ta/150 Å $Ti_{10}W_{90}$ (N) contacted by 3000 Å aluminium leads and surrounded by U-shaped focusing lines, both defined by lift-off. After the deposition of an oxide (Al_2O_3/SiO_2) passivation layer, a gold pad of 13 × 43 μm² was patterned on top of the bioactive sensors to define the area where the biological probes will immobilize. The biochip was wirebonded to a PCB carrier and the wires protected with silicon gel (Elastocil E41) to prevent it from corrosion during biological experiments.

The biochip readout starts by connecting the PCB to a portable measurement set-up that provides all the electronic circuitry to address and readout the sensors.[36]

A typical assay is performed by labeling the target molecules with streptavidin coated magnetic particles (ø250 nm, Nanomag, Micromod, Germany), magnetically concentrating it (down to 2 μL) and loading on the chip. Magnetic particles settling over the sensor promote a variation on the sensor resistance. After biomolecular recognition between probes and targets (~30 min) the unbound particles are washed out leaving a binding signal (Fig. 3).

In order to reduce the noise and the thermal drift of the sensors, the detection of the magnetic particles is made using a DC + AC external, in plane, transverse magnetic field (Fig. 2) to magnetize the particles. For our particular operational conditions and sensor geometry a 13.5 Oe rms + 30 Oe AC + DC field was used to obtain maximum signals. During the experiment the sensors are biased with a 1 mA current and sequentially addressed. Then, the signal is amplified with a gain of 40 and acquired at a sample rate of 844 samples per second. Finally, the acquired signal is digitally filtered with a 1 Hz bandwidth filter and the data are sent *via* Universal Serial Bus (USB) to a laptop.

Improvements at the level of hybridization efficiency, specific binding discrimination and detection limit were accomplished and detailed in ref. 37. The use of a magnetic focusing system on the hybridization of magnetically labeled target molecules (assisted hybridization by magnetic attraction) resulted in a better performance. In fact, the magnetic label that initially was identified as a limitation to passive hybridization reactions, decreasing its efficiency by about 50%, easily became an advantage when associated with an active transportation system. With the optimized focusing conditions of 40 mA DC on the lines and an external magnetic field of 30 Oe rms on the attraction system, the biological limit of detection (LOD) of the DNA-chip was significantly improved from picomolar down to the femtomolar range.

As target DNA sequences in clinical samples are found typically in minute quantities (<10^{-15} M), the actual limit of detection presented by the DNA-chip is approaching an adequate sensitivity, so it shows the potential to avoid the need for sample purification or amplification. Nevertheless, in cases where the LOD is affected by the complexity of real samples, a purification step can highly take advantage of the magnetic labeling of the molecules. Moreover, the magnetic carriers will further work as labels in the detection phase.

Additionally, in order to achieve a better control of the sample loading and washing steps during assay performance a microfluidic system was adapted to the biochip platform. The microfluidic channel was designed with a U-shape, 300 μm width, 100 μm height and a total length of ~9 mm to cover all the sensors on the chip. Results attained with the microfluidic system in comparison to the open chamber approach, besides improving the assay reproducibility, have reduced the time needed for magnetically labeled target molecules to reach the surface of the chip by about 60% (10 min compared to 30 min, respectively) (Fig. 4). This fact will cause the targets to start interacting earlier with the probes, which may be translated into shorter assay times. Furthermore, the detection signal for a target concentration of 1 pM has increased about three times when compared to the open chamber experiment, as depicted in Fig. 4.

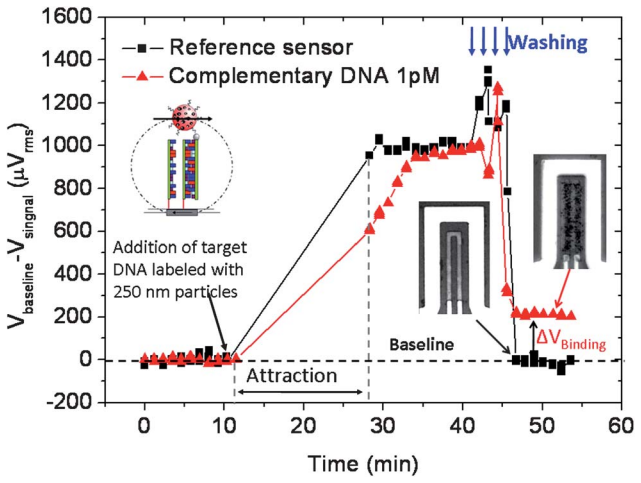

Fig. 3 Magnetic particles detection signal coming from two spin valve sensors (reference and probe-modified sensors) after 1 pM magnetically labeled target DNA addition, magnetic attraction, particle settling down and wash-out steps.

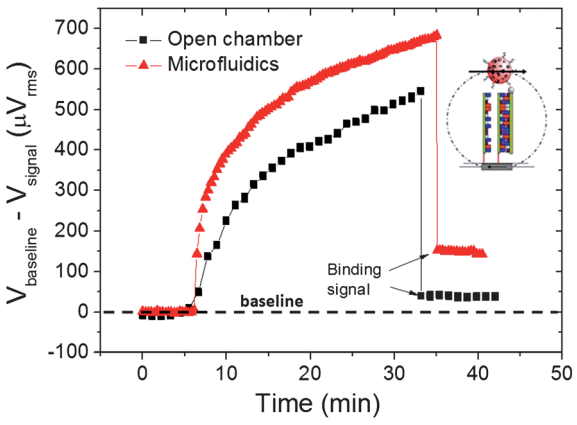

Fig. 4 Comparison between spin-valve sensor signals in a DNA hybridization detection assay at 1 pM concentration performed in a portable biochip-platform using a reactional open chamber (squares) or a microfluidic system (triangles).

 This journal is © The Royal Society of Chemistry 2012

View Article Online

Published on 07 December 2011. Downloaded by Universidade de Lisboa on 23/05/2017 15:50:11.

In conclusion, a magnetoresistive biochip was designed and used on a portable platform to detect biomolecular recognition. The detection of target DNA strands labeled with magnetic nanoparticles was further optimized by using on-chip attraction and focusing structures. Finally, the usage of microfluidics improved the detection time frame and signal amplitude in 60% and 3×, respectively. These biochip-based platforms are already at an advanced stage of development (prototyping level) for both DNA- and protein-chips and are expected to reach the market soon, as fully portable models for *in situ* usage. Meanwhile, other magnetoresistive platforms, further discussed in this paper, were developed aiming to solve other biological and biomedical challenges and are at a proof-of-concept level.

3. Magnetoresistive cytometer platforms

The detection of a specific cell using a magnetoresistive biochip as presented in the previous section was demonstrated in ref. 34. However, when studying suspended cells, it may be interesting to measure various physicochemical characteristics. For this purpose, fluorescent probes that stain cellular components or functions are used as reporters and introduced into a flow cytometer for detection.[38] In the past three decades, advances in precision technologies, dye synthesis and high-speed data-handling techniques have exerted synergistic effects on flow cytometry, bringing this powerful analytical tool into routine clinical and laboratory use in the field of cell/molecular biology,[39,40] disease diagnostics,[41,42] immunology,[43,44] genetics[45] and environmental monitoring.[46] In addition to detection and enumeration, some flow cytometers permit the separation and isolation of cells without loss of viability or particle purification without loss of characteristic structure.[47]

Although conventional state-of-the-art flow cytometry systems provide rapid and reliable analytical capacities, they are *bulky*, expensive and complex. Over the past decade, the drawbacks of conventional flow cytometers have encouraged efforts to take advantage of microfabrication technologies and advanced microfluidics to achieve smaller, simpler, more innovative and less expensive instrumentation with enhanced portability for on-site measurements.[48–67] Most of these microfabricated systems make use of solid-state devices (*e.g.* diode laser, P–I–N photodiode) to reduce the volume of the whole system but many still use external equipment for the detection and enumeration of cells/particles.

For the detection element of the micro-cytometers, many different options have been proposed, most of them using solid-state optical systems. The use of a diode laser and a single photon counting avalanche diode combined with digital data acquisition system to detect and count fluorescent beads flowing in a glass flow chamber at moderate rates was demonstrated.[68] Tung *et al.*[64] have chosen solid-state lasers and silicon-based P–I–N photodiode detectors combined with optical-fiber waveguides for multi-color laser excitation and fluorescence detection in a microfabricated flow cytometer made of PDMS. Work is still being done to improve the microfabrication of these elements (waveguides, optical fibers, lasers, diodes, *etc.*) and to reduce the size of the whole device, which is sometimes difficult due to external optical cameras commonly being used.

In this section, a new approach will be described in detail where the cytometer detection elements are integrated MR sensors, in this case spin valve sensors, that are used to count particles/magnetically labeled cells at high speed (cm s^{-1}).[7,17] Unlike external fluorescent/optical detectors, MR sensors are micro-fabricated and can be integrated within microfluidic channels. The magnetic labeling of cells has already been used in micro-cytometers but for pre-treatment steps not for detecting purposes.[69]

In this approach, a dynamic detection strategy where the magnetic labels are flowing inside the microchannels above the MR sensors was chosen (Fig. 5). This strategy has several advantages when comparing to the static one.[2,12,24,70] For example, there is no need to perform washing steps (avoiding false positives due to non specific bonding or false negatives due to excessive washing strength). Furthermore, the speed limit of the dynamic detection is not dependent on the spin valve response, but on the acquisition electronics.

In this case, a static magnetic field perpendicular to the sensor plane was used to magnetize cells labeled with super-paramagnetic nano-particles. This strategy was used in order not to affect the sensor response which would be the case if the field was in the plane of the spin valve, in the width direction.

One important parameter when using this technique to count cells is the total magnetic moment of the labelled cells. This value depends on the number of particles labelling the cells and their individual moment.

This type of magnetization and detection strategy gives origin to bipolar pulses, with the amplitude being dependent on the number of labels and on the cell height (Fig. 6).[17]

In order to measure the small signals arising from the flowing labeled cells, a commercial Stanford amplifier (SR560) set with a high pass filter at 100 Hz, a low pass filter at 3 kHz and a gain of

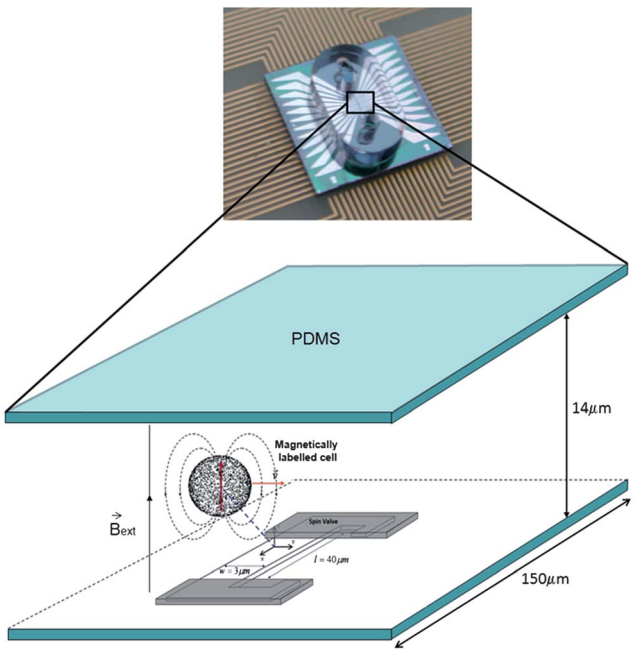

Fig. 5 Picture and schematic of the final chip and PDMS microfluidic platform showing the cell flowing above the spin valve sensor and the magnetic field lines due to the magnet placed below the chip/PCB.

View Article Online

Published on 07 December 2011. Downloaded by Universidade de Lisboa on 23/05/2017 15:50:11.

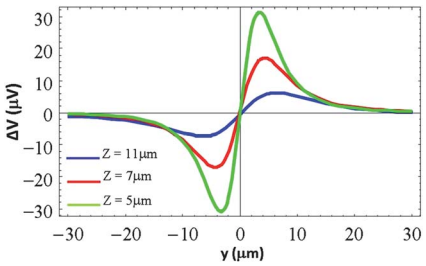

Fig. 6 Simulated signals for 5 μm diameter cells, labelled with 2880 uniformly distributed nanoparticles, vertically magnetized, at different heights (5 μm, 7 μm and 11 μm).

86 dB has been connected to the MR sensor. The output is then acquired on a computer through a commercial digital to analogue conversion board (Data Translation, 16 bit DAC) using an acquisition program that allows continuous acquisition up to a sample rate of 20 kHz. With this setup, the noise amplitude of the measurement is 4.5 μVrms for a bandwidth of 5 kHz and a sensor biasing current of 1 mA provided by a battery box. This corresponds to field equivalent noise of 0.9 μTrms. The sampling frequency of the acquisition has been chosen to be 5 kHz in order to provide a good temporal resolution of the signal. With this level of noise all cells flowing inside the channel can be detected, independently of their distance to the sensors.

First results were obtained with kg1-a cells (average diameter of 5 μm) labeled with CD34 MicroBeads (MACS, Miltenyi) having an overall diameter of about 50 nm. These cells are labeled on average with 2800 of these particles. Experiments were performed with 3 μm × 40 μm spin valve sensors (substrate/Ta (2.0)/$Ni_{80}Fe_{20}$(2.5)/$Co_{80}Fe_{20}$(2.5)/Cu(2.0)/$Co_{80}Fe_{20}$(2.5)/$Mn_{76}Ir_{24}$(6.0)/Ta(2.0)/TiW(N_2)(15), compositions in %). The cells were diluted in phosphate buffer solution (100 mM, pH 7.4) to a concentration of 4.76×10^3 cells per μL and inserted inside a 150 μm wide and 14 μm thick microchannel at speeds around 1 cm s^{-1}. For this experiment signal amplitudes (0-p) varied between 5 and 20 μV having the expected pulse shape (as visible in Fig. 7).

Counting processing was performed to evaluate the efficiency of this approach. Since each sensor is only 40 μm long, the device has been designed with three sensors covering the total width of the microfluidic channel. These sensors can be measured in a synchronous way. For high concentration and uniform samples (like the one stated here) it can be assumed that each sensor detects 27% of the total amount of cells passing through the channels. Therefore, the total number of cells can be extrapolated from the cell counts made with the middle sensor. Three runs of the same cell sample were achieved and compared with the hemocytometer results for the same sample.[25] As observed in Fig. 8, the results obtained on each run were found to be in good agreement with the hemocytometer results, confirming the correctness of the extrapolation.[25]

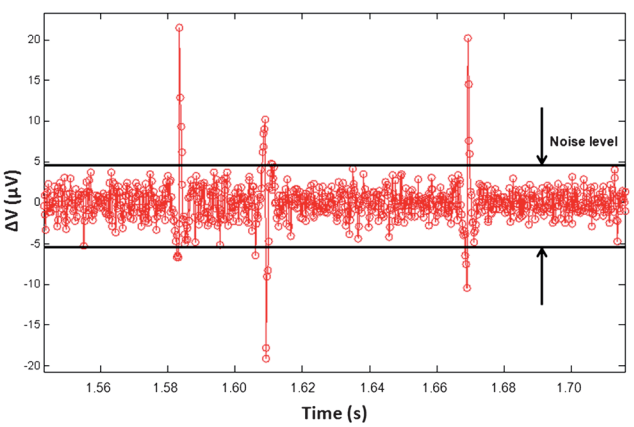

Fig. 7 Three single cell detection by a spin valve with 1 mA biasing current. The signal's amplitude is around 17–20 μV and the noise's amplitude approximately 3.54 μV_{rms}.

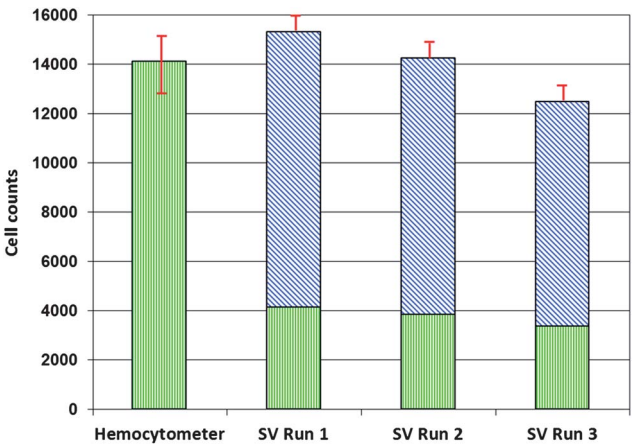

Fig. 8 Comparison between the cell counts obtained with the hemocytometer and with the magnetoresistive chip. With the hemocytometer, the cell counts of the 3.6 μL sample measured were estimated in 14 119, with the SV sensor the same sample was estimated to have 15 344, 14 274 and 12 496 cells (striped bars corresponding to the extrapolated values), leading to an average number of 14 037 cells. The filled bars correspond to the counts obtained with the SV prior to the extrapolation.

At the moment, the error of the spin valve counting only comes from the software and therefore it can be further improved although it is already lower than the hemocytometer one.

In this section, an integrated flow cytometer based on a spintronic device was developed and its capability of detecting a sample with a large concentration of magnetically labeled kg1-a cells was demonstrated. In the future, low concentration samples will be injected in the device and the measurement will be achieved using the synchronous detection of the three spin valve sensors. This flow cytometer can be further integrated with a microfluidic separation platform enabling the extraction and counting of CD34+ magnetically labelled cells coming from a real population of bone marrow or cord blood samples where the percentage of cells is very low.

4. Single molecule actuation and detection platforms

Manipulation techniques at the single molecule level with pN scale forces and measurement of displacements with 1 nm resolution are required for *in vitro* studies of individual molecular motors.[71–74] Molecular motors, such as DNA enzymes, bind to DNA and by pulling or twisting it they modify its length. These

 This journal is © The Royal Society of Chemistry 2012

View Article Online

Published on 07 December 2011. Downloaded by Universidade de Lisboa on 23/05/2017 15:50:11.

motors can generate maximum forces of tens of pN used to stretch single DNA molecules traveling a few base pairs (~1 nm) during an enzymatic cycle. This activity can be characterized by monitoring the end-to-end distance of the DNA stretched. Typically, a single molecule is attached between a surface and a force probe (*e.g.* a magnetic bead).

The main techniques allowing the manipulation of single molecules are optical tweezers,[75] where a dielectric bead is actuated with a laser. Magnetic tweezers using permanent magnets to create a magnetic force on a superparamagnetic bead,[76–85] atomic force microscopy based on the movement of the cantilever[86] or the surface with a piezoelectric element, microneedles[87,88] and biomembrane[89] force probes together with a suction pipette have been more recently introduced. Magnetic tweezers compared with the atomic force microscopy and optical systems present a larger range of force, stable and uniform without the need of feedback systems to impose constant amplitude. In addition, the manipulation is based on noncontact actuation and, since the solutions are hardly magnetic, higher signal to noise ratios can be obtained.

To measure the molecule end-to-end length we suggest the usage of a MR sensor to detect the vertical movement of a superparamagnetic bead by measuring its fringe field variation. The magnetic particle is further used in combination with magnetic tweezers based on a current loop to stretch a DNA strand (Fig. 9(a)).[11,90] Alternatively to the optical readout which requires a microscope, this approach allows an electrical readout with high throughput capability.[91] On-chip current loops with $\phi = 14 \pm 0.1$ μm of inner diameter were microfabricated on top of a baked photoresist mesa 4.5 ± 0.2 μm thick (Fig. 9(a)). Applying a current to this loop, a magnetic field gradient is generated on a magnetic bead anchored to the well bottom through a single DNA molecule. The resulting vertical magnetic force stretches the molecule. On a 3 μm (in diameter) magnetic bead, the resulting average vertical magnetic force generated by a 40 mA current applied to the loop is $F = 1.0 \pm 0.3$ pN along the z axis. As already presented in the first section, spin-valve sensors have been used in biochip applications. These sensors are only sensitive to an in-plane field, transverse to the sensor length. In this platform, tapered current lines parallel to the sensor stripe were included to generate an ac magnetizing field on the bead. At the sensor level, the field produced has only a vertical component. At the bead level, a longitudinal magnetic field component is created enabling the generation of a longitudinal bead fringe field which will be detected by the sensor.

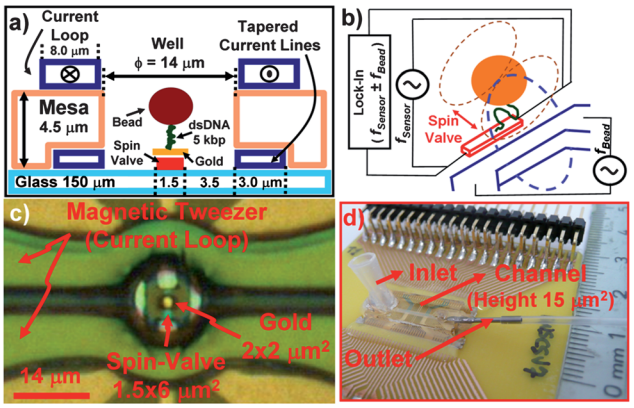

Fig. 9 On-chip magnetic tweezers integrated with a magnetoresistive sensor and a PDMS chamber (inset). (a) Cross-section schematic, (b) magnetic bead excitation and detection schematic, (c) microscope top view image of the detection cell focused on sensor plane and (d) microfluidic chamber.

The sensors were prepared by ion beam deposition (IBD) (Nordiko 3600 system)[92] and micro-fabricated with a dimension of 1.5 × 20 μm² (with a distance between leads of 1.5 × 6 μm²) using direct write laser lithography and ion beam milling.

The sensor leads and tapered current lines consist of magnetron sputtered $Al_{98.5}Si_{1.0}Cu_{0.5}$ 3000 Å/$Ti_{10}W_{90}$(N) 150 Å and $Al_{98.5}Si_{1.0}Cu_{0.5}$ 1.5 μm thick layers, respectively. Both structures were defined by photolithography and lift-off. The vertical separation between the sensor and the current loop is achieved with a cured 4.5 ± 0.2 μm thick photoresist deposited on top of the sensor. The detection and actuation systems are protected from corrosion using sputtered oxide (AlOx, SiO_2) and nitride layers (AlN), with a 3 layer structure of Al_2O_3 2000 Å/AlN 2000 Å/SiO_2 2000 Å. In order to establish an attachment region to specifically bind DNA, a 2 × 2 μm² gold pad (Cr 50 Å/Au 200 Å) is deposited by sputtering and defined by photolithography and lift-off on top of the passivation. Fig. 9(c) shows the top view of the tweezers and well. Finally, to confine the solution to the sensing region a PDMS based chamber is bonded to the chip surface (SiO_2). The channel has dimensions of 10 × 1 mm² and height 15 μm. Fig. 9(d) shows the fluidic chamber and the PCB holder where the final chip was wire-bonded.

Double stranded DNA (dsDNA) with 5 kbp (DNA length = 1.5 μm) modified with thiol (–SH) groups and biotin at opposite ends was used to anchor magnetic FeOx beads coated with streptavidin (Miromer-M, diameter $\phi = 3$ μm) on the gold pad surface.

The bead anchored moves due to tweezers actuation (Fig. 10 (a)) with a dc current $I_{MT} = 40$ mA creating a vertical magnetic force on the bead $F \approx 1.0$ pN. Fig. 10(b) shows a sequential run of the movement of an anchored bead during vertical actuation. When the bead is at an upper position ($I_{MT} = 40$ mA) a change in the diameter and intensity of bead diffraction pattern is observed.

Spin-valve sensors with field sensitivity $S = 0.06\%$/Oe (RAP = 128 Ω, RP = 122 Ω) were used. The tapered current lines biased with an AC current $I_{Tapered} = 54\ mA_{rms}$ induce an AC magnetic moment in the bead at frequency $f_B = 631$ Hz, see Fig. 9(b). To avoid capacitive coupling in the sensor readout, the sensor bias current is also modulated at frequency $f_S = 12.5$ kHz with an amplitude $I_B = 2.0\ mA_{pp}$. The bead creates a transverse in-plane AC field at the sensor level. The sensor output presents components at $f_B \pm f_S$. The signal is acquired with a Lock-In Amplifier at one frequency $f = 13\,131$ Hz, with an acquisition averaging time of $\Delta T = 100$ ms.

Fig. 11(a) shows the sensor output when a single bead is placed on top of the sensor at minimum separation, and then the bead is removed from the sensor surface using hydrodynamic force (increasing the flow rate). The sensor output with the bead over the sensor is $\Delta V = 8.7\ \mu V_{rms}$ with noise 0.4 μV_{rms}. As a result, a signal-to-noise ratio of SNR = 22 is achieved in the detection of a single bead in a no flow regime.

View Article Online

Published on 07 December 2011. Downloaded by Universidade de Lisboa on 23/05/2017 15:50:11.

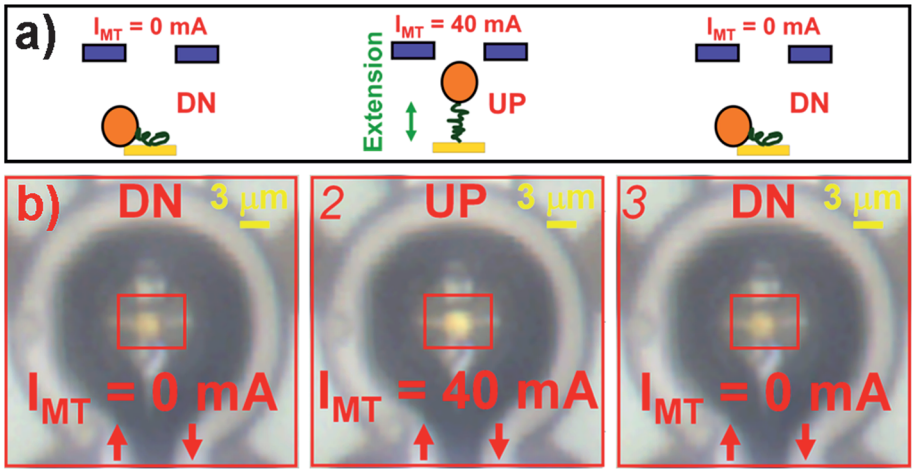

Fig. 10 (a) Schematic of the tweezers operation and bead levitation. (b) Optical view of the sensor region during bead vertical actuation driven by the magnetic tweezers.

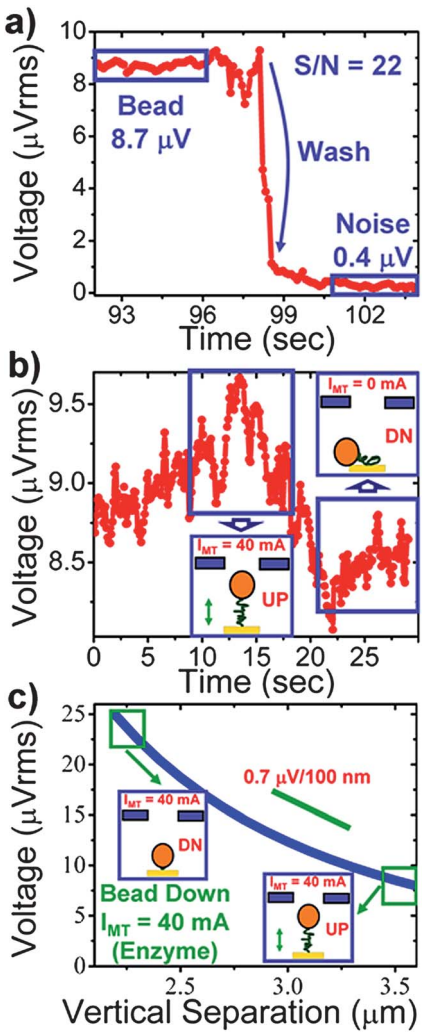

Fig. 11 (a) Bead presence signal measure at $f = f_S + f_B$. (b) Sensor output change during bead vertical actuation driven by the current loop. (c) Estimated sensor output for a biological bead actuation in a steady loop current.

Fig. 11(b) shows the sensor output when the dsDNA is stretched, by applying a force on the bead using the magnetic tweezers. The bead is centered with the sensor and the DNA is anchored on the gold pad. A force $F \approx 1.0$ pN corresponding to a current in the loop of IMT = 40 mA will stretch DNA to almost its total extension: $l \approx 1.26$ μm (total extension $l_{DNA} = 1.5$ μm (5 kbp)), corresponding to a fraction $\xi = l/l_{DNA} \approx 0.84$ given by the worm-like chain (WLC) model of DNA elasticity.

When the bead is at the lower position ($I_{MT} = 0$ mA), the moment of the bead only depends on the magnetizing field created by the tapered current lines. The sensor output in this case is $\Delta V_{DOWN} = 8.7 \pm 0.4$ μV_{rms} (Fig. 11(b)), at minimum separation, $z_{min} \approx 2.20$ μm (center of the bead-sensor distance). On the other hand, when the bead is pulled-up to a position $z \approx 3.46$ μm (center of the bead-sensor distance) actuated by the magnetic tweezers, the moment of the bead depends also on the vertical field created by the current loop. Increasing the current on the loop to IMT = 40 mA displaces the bead and in this case, the sensor output is $\Delta V_{UP} = 9.3 \pm 0.4$ μV_{rms}, corresponding to an individual bead susceptibility increase by a factor of 2.7.[9]

In Fig. 11(c) is represented the expected sensor output for the bead fringe field as a function of the vertical separation in a tweezers steady current regime ($I_{MT} = 40$ mA) fitting the sensor output observed in Fig. 11(b). In this regime, if the DNA's extension is reduced by the action of a DNA molecular motor (*e.g.* FtsK[93,94]) where the bead is pulled down, the sensor output change corresponds to the curve in Fig. 11(c), under constant magnetic tweezers force. The estimated resolution in the detection of the vertical displacement caused by motor activity is 60 nm considering the setup noise level and the slope 0.7 μV/100 nm of the curve in Fig. 11(c).

In conclusion, on-chip magnetic tweezers were integrated with magnetoresistive sensors producing forces up to 1.0 ± 0.3 pN capable of DNA stretching monitored in real time using spin-valve sensors. A bead vertical displacement resolution of 60 nm is derived for DNA molecular motor activity in a tweezers steady current regime. The system developed can be used to characterize real-time DNA–enzyme interaction at the single molecule level.

 This journal is © The Royal Society of Chemistry 2012

View Article Online

Published on 07 December 2011. Downloaded by Universidade de Lisboa on 23/05/2017 15:50:11.

This device is at the proof-of-concept level and many improvements may be envisaged on the increase of vertical displacement resolution. This could be assessed by increasing the sensor sensitivity (by using a magnetic tunnel junction sensor) and reducing the sensor noise by increasing its dimension. Furthermore, using a reference sensor will enable a differential measurement and therefore a more sensitive detection. Finally, a single molecule actuation and detection platform prototype will be developed including matrix based magnetoresistive sensors with improved resolution and multiplexed acquisition.

5. Biomedical signal detection platforms

5.1. Action potential detection

In the recent years, multiple techniques have been used to study the behavior and response of different brain areas to external stimuli in order to understand how the brain works. One of the most studied areas is the hippocampus, a structure of the limbic system that plays the most important role in memory.

Different techniques are currently used to study the behavior of the hippocampus. For example, the neuroscience group at Instituto de Medicina Molecular (IMM—in the medicine faculty of Lisbon) investigates the cellular and molecular mechanisms involved in the fine-tuning of neuronal communication, and their consequences for plasticity, neuroprotection and cognition. They use an electrophysiology technique, field potential, to study the electrical properties of neurons in the hippocampus involving measurements of voltage variation or electrical current flow.[95–98]

Open gate field-effect transistors are also used on the measurement of signals coming from the cell body of the neurons. The Membrane and Neurophysics group of the Max Planck Institute of Biochemistry studies the electrical interfacing of semiconductors with living cells, in particular neurons. Cellular processes are coupled to microelectronic devices through the direct contact of cell membranes to semiconductor chips. They couple a brain-grown net to numerous closely packed transistors and stimulation spots, in order to study the distributed dynamics of the neuronal network.[99–101]

Another technique uses microelectrodes to perform electrophysiological studies on hippocampal slices. Multi-channel recordings of excitatory postsynaptic potential are performed enabling the study of the spatial distribution of long-term potentiation.[102]

The integration of an extracellular electrophysiology system with a microfabricated device comprising MR sensors to measure the magnetic response of neurons from a rat or mice hippocampus brain slice is depicted in this section.

The main idea is to detect the magnetic field created by the activation of action/synaptic potential sources with MR sensors located several tens of micrometres above those sources. This measurement gives the information of the currents passing through the neurons and is therefore complementary to electrical measurements which sense electrical potentials.

The micro-fabricated device was designed to incorporate an array of fifteen $3 \times 50\ \mu m^2$ (width $\times$ distance between electrical leads) spin-valve sensors in a recording chamber for submerged brain slices used in the extracellular electrophysiology system. The spin valves are fabricated by ion beam deposition.[92]

After the deposition, the sensors are defined by ion milling. A 3000 Å aluminium layer is further patterned by optical lithography and metal lift off defining the sensor leads. The sensors showed a resistance of 500 Ω and a sensitivity of 0.14%/Oe. The sensors are passivated with sputtered 2000 Å Al_2O_3/2000 Å AlNx to protect against corrosion caused by an artificial cerebrospinal fluid solution, used to keep the hippocampus brain slice alive during the experiments (Krebs solution (mM): 124 NaCl, 3 KCl, 1.25 NaH_2PO_4, 26 $NaHCO_3$, 1 $MgSO_4$, 2 $CaCl_2$, and 10 glucose previously gassed with 95% O2–5% CO_2, pH 7.4). To conclude the fabrication process, the micro-fabricated wafer is diced into individual chips which are wire-bonded to a ribbon flat cable.

The experiments are performed on a hippocampus slice (400 μm thin) taken from mice brain. This slice is placed on top of the MR chip which was previously integrated in a recording chamber (Fig. 12). The chip comprises alignment marks allowing the positioning of the brain slice on the region of interest. Fig. 12 (a) describes the relative position of the sensor array with respect to the hippocampus structure and the field detection direction while Fig. 12(b) describes a cross-section of the chip and the brain slice.

The stimulation (rectangular pulses of 0.1 ms every 10 s) is delivered through a bipolar concentric wire electrode placed on the Schaffer collateral commissural fibers in the stratum radiatum, CA3 region. The created stimulus propagates along these fibers until it reaches the CA1 pyramidal neurons region (Fig. 12 (a)). Since this region contains synapses, it is possible to record a population excitatory postsynaptic potential (pEPSP). The EPSP represents a depolarization at the postsynaptic membrane, demonstrating a transmission in the CA3–CA1 synapse. If the magnitude of the depolarization is sufficient to bring the pyramidal cell to threshold, it will fire one or more action potentials that will be released from the hippocampus. These action potentials correspond to a constant flow of electrical charges, hence generating a local magnetic field. These action potentials occur in the pyramidal cell bodies exactly under the location

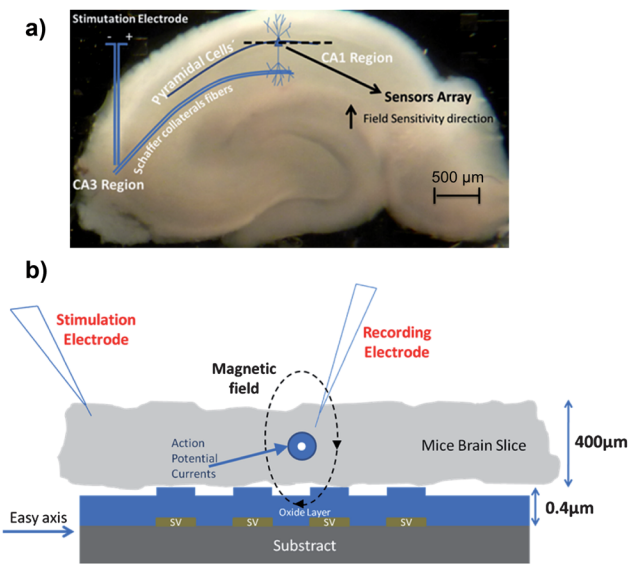

Fig. 12 MR device integrated in the recording chamber with a mice hippocampus brain slice placed on top of the MR sensors. (a) Top view microscopic picture. (b) Schematic representation of the transversal view.

View Article Online

Published on 07 December 2011. Downloaded by Universidade de Lisboa on 23/05/2017 15:50:11.

where the MR sensors were placed (spacing of about 1 μm due to the thickness of contacts and passivation layers). Therefore, the resultant magnetic field can be detected by the sensors.

In order to measure the small signals coming from the neurons, a signal amplifying system was used.[17] A commercial Stanford amplifier (SR560) set with a high pass filter at 30 Hz, a low pass filter at 100 kHz and a gain of 86 dB has been connected to the spin valve sensor. A sensor biasing current of 1 mA was provided by a battery. The output is then acquired by a commercial digital to analog conversion board (Data Translation, 16 bit DAC) and displayed on a computer. The system allows continuous acquisition up to a sample rate of 20 kHz.

Fig. 13 shows a sequence of pulses measured after hippocampus excitation by one of the spin valve sensors present in the linear array. The spin valve sensor readout consists of pulses of 20 μV of amplitude and a pulse length of 30 to 40 ms. The pulses were recorded only in the pyramidal bodies' cell region and are interpreted as coming from action potential currents generated by the activation of multiple pyramidal cells bodies. Considering a sensor sensitivity of 0.14%/Oe, the 20 μV amplitude signal corresponds to a magnetic field of 2.5 μTesla, for a 10 μm source-sensor separation. Considering a stratum pyramidal dimension of 130 μm[99] corresponding to the length of the axon where the action potential propagates and a sensor-action potential source distance of 10 μm, a single cell body generating an action potential creates an intracellular current of 50 nA,[103] which corresponds to a magnetic field created on the sensor of 6.5 nTesla. Therefore, the measured pulse would require at least 500 cell bodies responding synchronously.

The type of signal shown in Fig. 13 could also arise from a capacitive coupling between the sensor leads and the brain slice, which is a highly resistive media with an incorporated voltage source (the action potential).

In order to separate real biological signals from spurious results, two experiments were performed (Fig. 14). On the first hand, a Glutamate post-synaptic receptor blocker (CNQX) that blocks the fast excitatory synaptic responses in the dendrites was applied. The same type of signal is observed in the sensor, discarding synapses as the source of the signal (Fig. 14(a)). On the second hand, a drug (TTX) was administered to block the sodium channels, which are responsible for the generation of the action potentials in the cell body. As a consequence, the pulses measured on the sensors stopped, confirming that the acquired signals are coming from biological action potential sources (Fig. 14(b)).

In conclusion, the results attained with this new type of hybrid platform have proven that the signals obtained are biomagnetic. Efforts are being made to improve the current electronic system in terms of noise reduction and also to simultaneously address and acquire the whole sensor array. Moreover the sensitivity of magnetoresistive sensors can be increased in order to detect smaller magnetic fields, in future work MgO based magnetic tunnel junctions (sensitivity > 2%, resistance-area products R_A < 100 Ohm μm^2) will be used to fabricate ultra low field

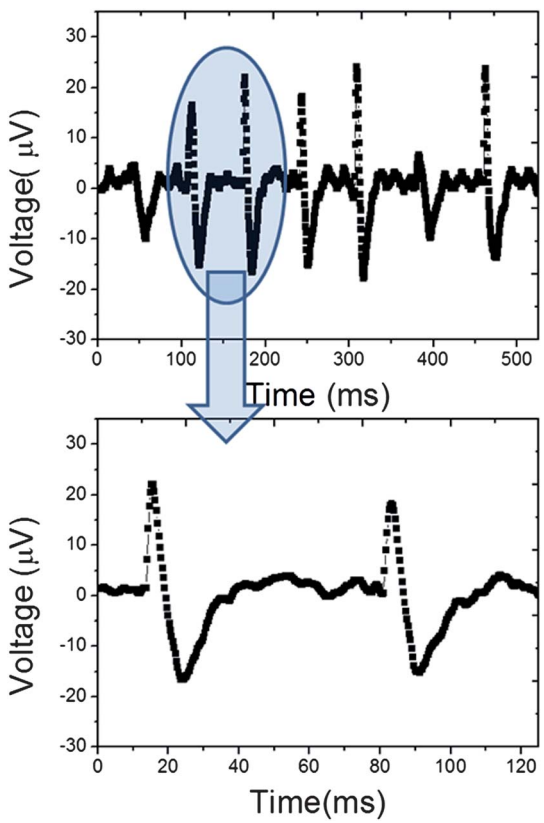

Fig. 13 The spin valve sensor readout and a close up of a signal with a 20 μV amplitude and a pulse length of around 30 ms.

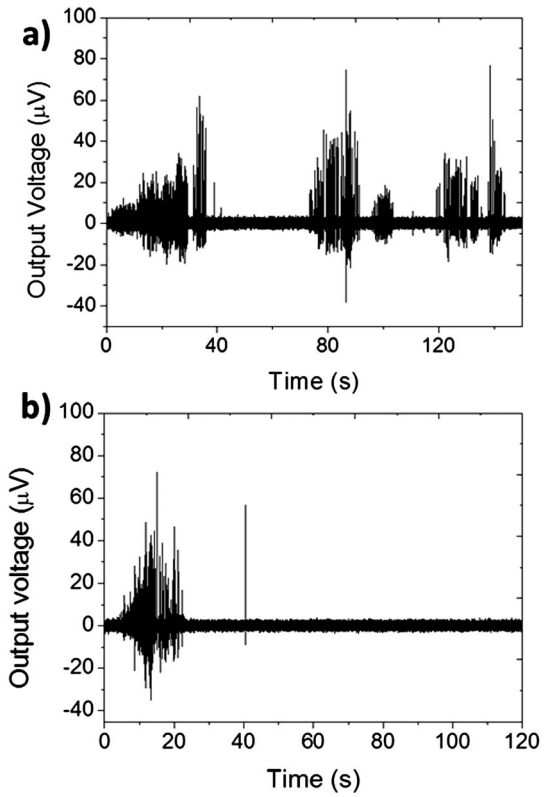

Fig. 14 (a) Spin valve sensor readout after applying CNQX drug, a synaptic response blocker and (b) spin valve readout after applying TTX drug, an action potential response blocker.

 This journal is © The Royal Society of Chemistry 2012

View Article Online

Published on 07 December 2011. Downloaded by Universidade de Lisboa on 23/05/2017 15:50:11.

detectors. Also the integration of these magnetoresistive sensors (magnetic tunnel junction or spin valve) inside a silicon needle probe will allow the direct detection of the magnetic field generated by the neurons. Metallic microelectrodes will be included inside the needles to provide the local excitation ability. In sum, the detection of signals from synaptic sources may be possible increasing the capabilities of this hybrid platform allowing the improvement of the electrophysiological studies (analysis of magnetic/electrical brain activity in great detail).

5.2. Magneto-cardiography

The platform presented previously for the detection of action potential on a brain slice is of great importance for fundamental studies related with neuron to neuron signal propagation. Nevertheless, from a medical diagnostic point of view, the usage of this platform would require surgery and therefore it would be an invasive diagnostic instrument.

To overcome this limitation, there is an increasing interest in using MR-based platforms for non-invasive detection of biomagnetic signals. The two most studied biomagnetic signal sources are the heart and the brain. The magnetic field amplitude generated by these two systems is of the order of 1 pT and 50 fT, respectively, for the signals from the heart at the skin level and from the electric currents flowing in active nerve cells in the brain. Since these signals are far below the magnetic field of the earth ($\sim 10^{-4}$ T), the development of these detection systems is challenging. However, their detection would allow a non-invasive study and disease diagnostics in the brain or heart, thus representing a high impact in health care.

The most sensitive commercial systems for both magnetoencephalography (MEG)[104] and magnetocardiography (MCG)[105] use extremely sensitive superconducting quantum interference devices (SQUIDs), capable to detect down to 10^{-15} Tesla with noise levels of 1 fT $Hz^{-1/2}$. SQUIDs are very sensitive flux magnetometers based on the Josephson effect, a quantum superconducting effect and therefore need to work at low temperatures. This is a major disadvantage since the temperature reduction involves a large apparatus which may not always be comfortable for the patient, and is very limiting in terms of portability. Furthermore, since SQUIDs detect a magnetic flux and not a magnetic field (thus averaging magnetic field sources over large areas in space), reducing their size to increase the system spatial resolution would compromise the sensitivity.

Therefore, recently new magnetic field sensor technologies have been proposed to overcome SQUID limitations. For example, fiber sensors operating at room temperature,[106] and spin exchange relaxation-free atomic magnetometers[107] offer detection sensitivities comparable to or exceeding cryogenic SQUID technology.

A hybrid technology was proposed by Pannetier-Lecoeur,[108] where an MR sensor is integrated with a high temperature superconductor (YBCO) flux-to-field transformer (Fig. 15(a). The use of GMR sensors allows the direct detection of magnetic fields at room temperature and can be designed down to the nanometre scale (allowing an increase in spatial resolution). When a superconducting loop containing a constriction is coupled to these GMR sensors an increase in sensitivity is obtained. The final device is incorporated in a small, portable

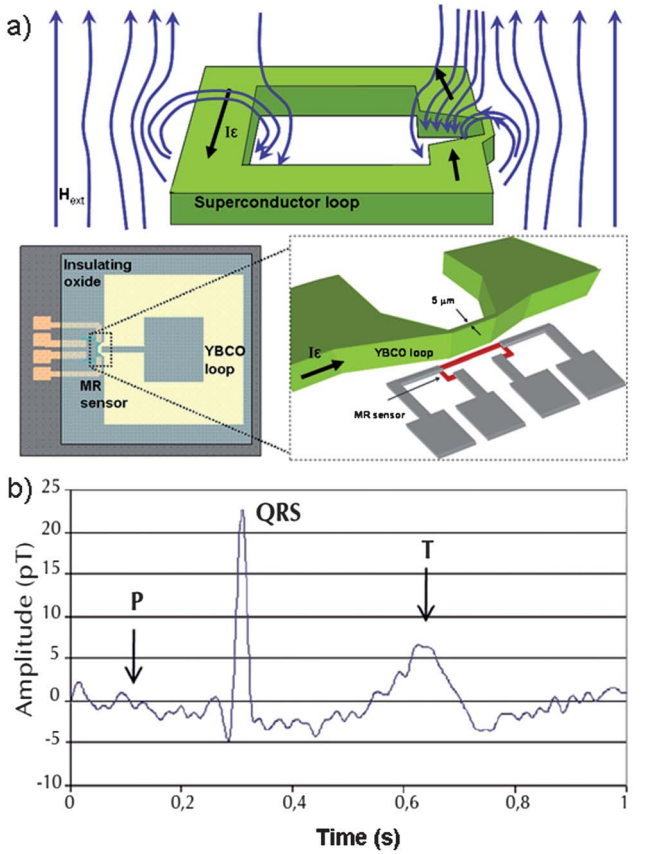

Fig. 15 (a) Schematic representation of the mixed sensor, comprising the large superconductor loop. (b) Magneto-cardio signal measured with a mixed sensor. The pattern signal resembles those obtained with conventional electrocardiography techniques [courtesy of Pannetier-Lecoeur, CEA].

Dewar, required for low temperature operation of the superconductor. The device thermal noise levels of few fT $Hz^{-1/2}$ obtained now are comparable to those measured with low-Tc SQUID, with small dependence on the frequency. An example of signal obtained by these sensors when used in magneto-cardiography is shown in Fig. 15(b).

In the measured magneto-cardiogram, the typical components (the P-wave, the QRS complex and the T-wave) of a normal electrocardiogram are observed. Therefore, although still at the proof-of-concept level, the magneto-cardiography technique using MR sensors integrated on hybrid devices showed very promising results as a sensitive and non-invasive diagnostic method. The presented system still requires a dewar for cooling the superconducting flux transform. This cooling system will be further integrated in order to obtain a more handy system. Another approach that is being investigated is to replace the superconducting flux transform by a hybrid system integrating magnetic flux concentrator (working at room temperature) with micro-electromechanical systems (MEMS).

6. General conclusion

Integrated spintronic platforms are being actively investigated aiming application at different biomedical topics. Some of those

View Article Online

Published on 07 December 2011. Downloaded by Universidade de Lisboa on 23/05/2017 15:50:11.

topics were herein discussed; namely biochip-based platforms (DNA- and protein-chips) for detection of biomolecular recognition; microfluidic platforms for cell separation and counting (flow cytometry); neuroelectronic and magneto-cardiology devices for acquisition of brain and heart biomagnetic signals; and lab-on-a-chip type platforms for single molecule actuation and detection (magnetic tweezers).

Most of these platforms consist of a microfluidic unit where the bioassay/biological measurement takes place, a sensing chip comprising electrical microfabricated structures (*e.g.* current lines, magnetic tweezers) and integrated magnetoresistive sensors (*e.g.* spin-valves), and electronic control and readout boards.

In the biochip platforms, diverse formats of magnetoresistive sensors are being used to optimize the detection of biomolecular recognition events, where target molecules are labeled with nanometric or micron sized magnetic particles. Target molecules may be detected statically by immobilized probes over the sensing sites or dynamically in flow inside microfluidic channels. In the latter case, spin valve sensors were used to count magnetic particles or magnetically labeled cells at high speed (cm s^{-1}).

For single molecule studies on-chip magnetic tweezers were integrated with magnetoresistive sensors producing forces up to 1.0 ± 0.3 pN capable of magnetic bead actuation. The system developed can be used to characterize real-time bio-interaction at the single molecule level. In particular, the vertical displacement of a DNA strand tagged with a magnetic bead, derived from the activity of a molecular motor, can be followed with a resolution of 60 nm.

Additionally, for biomedical imaging applications, field sensitivity is being pushed below 1 pT $Hz^{-1/2}$ in hybrid devices incorporating flux guides with the magnetoresistive element. The use of GMR sensors allows the direct detection of magnetic fields (from brain and heart) at room temperature and can be designed down to the nanometre scale, allowing an increase in spatial resolution.

Most of the presented spintronic platforms, with the exception of biochip-based platforms, still are at a proof-of-concept level. Nevertheless, the enormous potential of these platforms foresees great advances in biomedical instrumentation in the next decades. Furthermore, improvements in the existing devices and the emergence of novel ones applied to other biomedical areas are just a matter of time.

References

1 J. Germano, V. Martins, F. Cardoso, T. Almeida, L. Sousa, P. Freitas and M. Piedade, *Sensors*, 2009, **9**, 4119–4137.
2 B. M. de Boer, J. A. H. M. Kahlman, T. P. G. H. Jansen, H. Duric and J. Veen, *Biosens. Bioelectron.*, 2007, **22**, 2366–2370.
3 R. S. Gaster, D. A. Hall and S. X. Wang, *Lab Chip*, 2011, **11**, 950–956.
4 B. Dieny, *Spin Valves*, Elsevier, Amsterdam, 2004.
5 J. Amaral, S. Cardoso, P. P. Freitas and A. M. Sebastião, *J. Appl. Phys.*, 2011, **109**, 07B308.
6 M. Pannetier-Lecoeur, L. Parkkonen, N. Sergeeva-Chollet, H. Polovy, C. Fermon and C. Fowley, *Appl. Phys. Lett.*, 2011, **98**, 153705.
7 J. Loureiro, C. Fermon, M. Pannetier-Lecoeur, G. Arrias, R. Ferreira, S. Cardoso and P. P. Freitas, *IEEE Trans. Magn.*, 2009, **45**, 4873–4876.
8 D. L. Graham, H. Ferreira, J. Bernardo, P. P. Freitas and J. M. S. Cabral, *J. Appl. Phys.*, 2002, **91**, 7786.
9 G. X. Li, S. H. Sun, R. J. Wilson, R. L. White, N. Pourmand and S. X. Wang, *Sens. Actuators, A*, 2006, **126**, 98–106.
10 W. Schepper, J. Schotter, H. Brückl and G. Reiss, *J. Biotechnol.*, 2004, **112**, 35–46.
11 R. C. Chaves, D. Bensimon and P. P. Freitas, *J. Appl. Phys.*, 2011, **109**, 064702.
12 D. L. Graham, H. A. Ferreira and P. P. Freitas, *Trends Biotechnol.*, 2004, **22**, 455–462.
13 L. Xu, H. Yu, M. S. Akhras, S.-J. Han, S. Osterfeld, R. L. White, N. Pourmand and S. X. Wang, *Biosens. Bioelectron.*, 2008, **24**, 99–103.
14 V. C. Martins, F. A. Cardoso, J. Germano, S. Cardoso, L. Sousa, M. Piedade, P. P. Freitas and L. P. Fonseca, *Biosens. Bioelectron.*, 2009, **24**, 2690–2695.
15 C. R. Tamanaha, S. P. Mulvaney, J. C. Rife and L. J. Whitman, *Biosens. Bioelectron.*, 2008, **24**, 1–13.
16 B. Srinivasan, Y. Li, Y. Jing, Y. Xu, X. Yao, C. Xing and J. Wang, *Angew. Chem., Int. Ed.*, 2009, **48**, 2764–2767.
17 J. Loureiro, R. Ferreira, S. Cardoso, P. P. Freitas, J. Germano, C. Fermon, G. Arrias, M. Pannetier-Lecoeur, F. Rivadulla and J. Rivas, *Appl. Phys. Lett.*, 2009, **95**, 034104.
18 T. Vo-Dinh and B. Cullum, *Fresenius' J. Anal. Chem.*, 2000, **366**, 540–551.
19 M. Megens and M. Prins, *J. Magn. Magn. Mater.*, 2005, **293**, 702–708.
20 S. P. Mulvaney, K. M. Myers, P. E. Sheehan and L. J. Whitman, *Biosens. Bioelectron.*, 2009, **24**, 1109–1115.
21 F. A. Cardoso, H. A. Ferreira, J. P. Conde, V. Chu, P. P. Freitas, D. Vidal, J. Germano, L. Sousa, M. S. Piedade, B. A. Costa and J. M. Lemos, *J. Appl. Phys.*, 2006, **99**, 08B307.
22 F. A. Cardoso, J. Germano, R. Ferreira, S. Cardoso, V. C. Martins, P. P. Freitas, M. S. Piedade and L. Sousa, *J. Appl. Phys.*, 2008, **103**, 07A310.
23 D. L. Graham, H. A. Ferreira, P. P. Freitas and J. M. S. Cabral, *Biosens. Bioelectron.*, 2003, **18**, 483–488.
24 S. X. Wang, S.-Y. Bae, G. Li, S. Sun, R. L. White, J. T. Kemp and C. D. Webb, *J. Magn. Magn. Mater.*, 2005, **293**, 731–736.
25 V. C. Martins, J. Germano, F. A. Cardoso, J. Loureiro, S. Cardoso, L. Sousa, M. Piedade, L. P. Fonseca and P. P. Freitas, *J. Magn. Magn. Mater.*, 2009, **322**, 1655–1663.
26 P. Yager, T. Edwards, E. Fu, K. Helton, K. Nelson, M. R. Tam and B. H. Weigl, *Nature*, 2006, **442**, 412–418.
27 R. De Palma, G. Reekmans, W. Laureyn, G. Borghs and G. Maes, *Anal. Chem.*, 2007, **79**, 7540–7548.
28 W. U. Dittmer, P. de Kievit, M. W. J. Prins, J. L. M. Vissers, M. E. C. Mersch and M. F. W. C. Martens, *J. Immunol. Methods*, 2008, **338**, 40–46.
29 K. Taton, D. Johnson, P. Guire, E. Lange and M. Tondra, *J. Magn. Magn. Mater.*, 2009, **321**, 1679–1682.
30 R. S. Gaster, L. Xu, S.-J. Han, R. J. Wilson, D. A. Hall, S. J. Osterfeld, H. Yu and S. X. Wang, *Nat. Nanotechnol.*, 2011, **6**, 314–320.
31 S. J. Osterfeld, H. Yu, R. S. Gaster, S. Caramuta, L. Xu, S. J. Han, D. A. Hall, R. J. Wilson, S. H. Sun, R. L. White, R. W. Davis, N. Pourmand and S. X. Wang, *Proc. Natl. Acad. Sci. U. S. A.*, 2008, **105**, 20637–20640.
32 Y. Li, B. Srinivasan, Y. Jing, X. Yao, M. A. Hugger, J.-P. Wang and C. Xing, *J. Am. Chem. Soc.*, 2010, **132**, 4388–4392.
33 H. A. Ferreira, D. L. Graham, N. Feliciano, L. A. Clarke, M. D. Amaral and P. P. Freitas, *IEEE Trans. Magn.*, 2005, **41**, 4140–4142.
34 S. A. M. Martins, V. C. Martins, M. T. B. F. Frasco, A. G. B. Castro, P. P. Freitas and L. P. Fonseca, *Proceedings of 7th Ibero-American Congress on Sensors (Ibersensor 2010)*, 2010, 1–7
35 H. A. Ferreira, N. Feliciano, D. L. Graham, L. A. Clarke, M. D. Amaral and P. P. Freitas, *Appl. Phys. Lett.*, 2005, **87**, 013901.
36 M. Piedade, L. A. Sousa, T. M. de Almeida, J. Germano, B. D. da Costa, J. M. Lemos, P. P. Freitas, H. A. Ferreira and F. A. Cardoso, *IEEE Trans. Circuits Syst. I: Regul.Pap.*, 2006, **53**, 2384–2395.
37 V. C. Martins, F. A. Cardoso, J. Germano, S. Cardoso, L. Sousa, M. Piedade, P. P. Freitas and L. P. Fonseca, *Biosens. Bioelectron.*, 2009, **24**, 2690–2695.

 This journal is © The Royal Society of Chemistry 2012

View Article Online

Published on 07 December 2011. Downloaded by Universidade de Lisboa on 23/05/2017 15:50:11.

38 H. M. Shapiro, *Using Flow Cytometers: Applications, Extensions, and Alternatives*, John Wiley & Sons, Inc., 2005.
39 C. L. Harding, D. R. Lloyd, C. M. McFarlane and M. Al-Rubeai, *Biotechnol. Prog.*, 2000, **16**, 800–802.
40 G. Boeck, in *International Review of Cytology*, Academic Press, 2001, vol. 204, pp. 239–298.
41 D. S. Stein, J. A. Korvick and S. H. Vermund, *J. Infect. Dis.*, 1992, **165**, 352–363.
42 D. Fenili and B. Pirovano, *Clin. Chem. Lab. Med.*, 1998, **36**, 909–917.
43 H. Gabriel and W. Kindermann, *Sports Med. (Auckland)*, 1995, **20**, 302–320.
44 G. Garratty and P. A. Arndt, *Cytometry*, 1999, **38**, 259–267.
45 N. Wedemeyer and T. Pötter, *Clin. Genet.*, 2001, **60**, 1–8.
46 G. B. J. Dubelaar, P. L. Gerritzen, A. E. R. Beeker, R. R. Jonker and K. Tangen, *Cytometry*, 1999, **37**, 247–254.
47 P. K. Horan and L. L. Wheeless, *Science*, 1977, **198**, 149–157.
48 R. Miyake, H. Ohki, I. Yamazaki and T. Takagi, *JSME Int. J., Ser. B*, 1997, **40**, 106–113.
49 D. Sobek, A. M. Young, M. L. Gray and S. D. Senturia, *Microfabricated Fused Silica Flow Chambers for Flow Cytometry*, 1993.
50 G.-B. Lee, C.-H. Lin and G.-L. Chang, *Sens. Actuators, A*, 2003, **103**, 165–170.
51 G. B. Lee, C. I. Hung, B. J. Ke, G. R. Huang, B. H. Hwei and H. F. Lai, *Trans. ASME I*, 2001, 672–679.
52 S. Gawad, L. Schild and P. Renaud, *Lab Chip*, 2001, **1**, 76–82.
53 E. Altendorf, D. Zebert, M. Holl and P. Yager, *Presented in Part at the International Conference on solid State Sensors and Actuators*, Chicago, IL, USA, 1997.
54 B. H. Weigl, R. Bardell, T. Schulte, F. Battrell and J. Hayenga, *Biomed. Microdevices*, 2001, **3**, 267–274.
55 S. D. H. Chan, G. Luedke, M. Valer, C. Buhlmann and T. Preckel, *Cytometry, Part A*, 2003, **55**, 119–125.
56 E. Cabuz, J. Schwichtenberg, B. DeMers, E. Satren, A. Padmanabhan and C. Cabuz, *MEMS-Based Flow Controller for Flow Cytometry*, 2002.
57 L.-K. Chau, T. Osborn, C.-C. Wu and P. Yager, *Anal. Sci.*, 1999, **15**, 721–724.
58 H.-T. Chen and Y.-N. Wang, *Microfluid. Nanofluid.*, 2008, **5**, 689–694.
59 S. Chung, S. J. Park, J. K. Kim, C. Chung, D. C. Han and J. K. Chang, *Microsyst. Technol*, 2003, **9**, 525–533.
60 D. Huh, A. H. Tkaczyk, J. H. Bahng, Y. Chang, H.-H. Wei, J. B. Grotberg, C.-J. Kim, K. Kurabayashi and S. Takayama, *J. Am. Chem. Soc.*, 2003, **125**, 14678–14679.
61 D. Huh, Y.-C. Tung, H.-H. Wei, J. B. Grotberg, S. J. Skerlos, K. Kurabayashi and S. Takayama, *Biomed. Microdevices*, 2002, **4**, 141–149.
62 M. A. McClain, C. T. Culbertson, S. C. Jacobson, N. L. Allbritton, C. E. Sims and J. M. Ramsey, *Anal. Chem.*, 2003, **75**, 5646–5655.
63 M. A. McClain, C. T. Culbertson, S. C. Jacobson and J. M. Ramsey, *Anal. Chem.*, 2001, **73**, 5334–5338.
64 Y.-C. Tung, M. Zhang, C.-T. Lin, K. Kurabayashi and S. J. Skerlos, *Sens. Actuators, A*, 2004, **98**, 356–367.
65 S. Kostner and M. J. Vellekoop, *Sens. Actuators, A*, 2008, **132**, 512–517.
66 Y.-C. Tung, Y.-s. Torisawa, N. Futai and S. Takayama, *Lab Chip*, 2007, **7**, 1497–1503.
67 S. Joo, K. H. Kim, H. C. Kim and T. D. Chung, *Biosens. Bioelectron.*, 2010, **25**, 1509–1515.
68 S. Niehren, W. Kinzelbach, S. Seeger and J. Wolfrum, *Anal. Chem.*, 1995, **67**, 2666–2671.
69 S.-Y. Yang, K.-Y. Lien, K.-J. Huang, H.-Y. Lei and G.-B. Lee, *Biosens. Bioelectron.*, 2008, **24**, 855–862.
70 D. R. Baselt, G. U. Lee, M. Natesan, S. W. Metzger, P. E. Sheehan and R. J. Colton, *Biosens. Bioelectron.*, 1998, **13**, 731–739.
71 E. A. Abbondanzieri, W. J. Greenleaf, J. W. Shaevitz, R. Landick and S. M. Block, *Nature*, 2005, **438**, 460–465.
72 W. J. Greenleaf and S. M. Block, *Science*, 2006, **313**, 801.
73 M. D. Wang, M. J. Schnitzer, H. Yin, R. Landick, J. Gelles and S. M. Block, *Science*, 1998, **282**, 902–907.
74 H. Yin, M. D. Wang, K. Svoboda, R. Landick, S. M. Block and J. Gelles, *Science*, 1995, **270**, 1653–1657.
75 A. Ashkin, J. M. Dziedzic, J. E. Bjorkholm and S. Chu, *Opt. Lett.*, 1986, **11**, 288–290.
76 G. Charvin, T. R. Strick, D. Bensimon and V. Croquette, *Annu. Rev. Biophys. Biomol. Struct.*, 2005, **34**, 201–219.
77 C. Gosse and V. Croquette, *Biophys. J.*, 2002, **82**, 3314–3329.
78 W. J. Greenleaf, M. T. Woodside and S. M. Block, *Annu. Rev. Biophys. Biomol. Struct.*, 2007, **36**, 171–190.
79 T. Lionnet, A. Dawid, S. Bigot, F.-X. Barre, O. A. Saleh, F. Heslot, J.-F. Allemand, D. Bensimon and V. Croquette, *Nucleic Acids Res.*, 2006, **34**, 4232–4244.
80 K. C. Neuman, T. Lionnet and J.-F. Allemand, *Annu. Rev. Mater. Sci.*, 2007, **37**, 33–67.
81 R. Seidel, J. van Noort, C. van der Scheer, J. G. P. Bloom, N. H. Dekker, C. F. Dutta, A. Blundell, T. Robinson, K. Firman and C. Dekker, *Nat. Struct. Mol. Biol.*, 2004, **11**, 838–843.
82 T. R. Strick, J. F. Allemand, D. Bensimon and V. Croquette, *Biophys. J.*, 1998, **74**, 2016–2028.
83 T. R. Strick, V. Croquette and D. Bensimon, *Proc. Natl. Acad. Sci. U. S. A.*, 1998, **95**, 10579–10583.
84 J. Yan, D. Skoko and J. F. Marko, *Phys. Rev. E: Stat., Nonlinear, Soft Matter Phys.*, 2004, **70**, 011905.
85 T. R. Strick, J.-F. Allemand, D. Bensimon, A. Bensimon and V. Croquette, *Science*, 1996, **271**, 1835–1837.
86 A. Andrea and F. Paolo, *Meas. Sci. Technol.*, 2005, **16**, R65.
87 A. Ishijima, H. Kojima, H. Higuchi, Y. Harada, T. Funatsu and T. Yanagida, *Biophys. J.*, 1996, **70**, 383–400.
88 A. Kishino and T. Yanagida, *Nature*, 1988, **334**, 74–76.
89 E. Evans, K. Ritchie and R. Merkel, *Biophys. J.*, 1995, **68**, 2580–2587.
90 Patent, UK Intellectual Property Office, *Patent application number* 0918016.7 (14 October 2009), 2009.
91 http://www.picotwist.com/.
92 V. Gehanno, P. P. Freitas, A. Veloso, J. Ferreira, B. Almeida, J. B. Sousa, A. Kling, J. C. Soares and M. F. da Silva, *IEEE Trans. Magn.*, 1999, **35**, 4361–4367.
93 P. J. Pease, O. Levy, G. J. Cost, J. Gore, J. L. Ptacin, D. Sherratt, C. Bustamante and N. R. Cozzarelli, *Science*, 2005, **307**, 586–590.
94 O. A. Saleh, S. Bigot, F.-X. Barre and J.-F. Allemand, *Nat. Struct. Mol. Biol.*, 2005, **12**, 436–440.
95 A. M. Sebastiao, R. A. Cunha, A. de Mendonca and J. A. Ribeiro, *Br. J. Pharmacol.*, 2000, **131**, 1629–1634.
96 A. R. Costenla, A. de Mendonca and J. A. Ribeiro, *Brain Res.*, 1999, **851**, 228–234.
97 A. R. Costenla, L. V. Lopes, A. de Mendonca and J. A. Ribeiro, *Neurosci. Lett.*, 2001, **302**, 53–57.
98 J. A. Ribeiro, A. M. Sebastiao and A. de Mendonca, *Prog. Neurobiol.*, 2002, **68**, 377–392.
99 P. Fromherz, *1st International Ieee Embs Conference on Neural Engineering 2003, Conference Proceedings*, 2003, p. 1.
100 I. Peitz and P. Fromherz, *Eur. Phys. J. E: Soft Matter Biol. Phys.*, 2009, **30**, 223–231.
101 P. Fromherz, *Solid-State Electron.*, 2008, **52**, 1364–1373.
102 H. Oka, K. Shimono, R. Ogawa, H. Sugihara and M. Taketani, *J. Neurosci. Methods*, 1999, **93**, 61–67.
103 A. L. Hodgkin and A. F. Huxley, *J. Physiol.*, 1952, **117**, 500–544.
104 O. V. Lounasma and H. Seppa, *J. Low Temp. Phys.*, 2004, **135**, 295–335.
105 M. M. Budnyk, I. D. Voytovych, Y. D. Minov, P. G. Sutkovyi, M. A. Primin, I. V. Nedayvoda and V. V. Vasyliev, *Neurol. Clin. Neurophysiol.*, 2004, **2004**, 112.
106 T. G. Giallorenzi, J. A. Bucaro, A. Dandridge, G. H. Sigel, J. H. Cole, S. C. Rashleigh and R. G. Priest, *IEEE J. Quantum Electron.*, 1982, **18**, 626–665.
107 S. Knappe, T. H. Sander, O. Kosch, F. Wiekhorst, J. Kitching and L. Trahms, *Appl. Phys. Lett.*, 2010, **97**, 133703.
108 M. Pannetier-Lecoeur, C. Fermon, G. Le Goff, J. Simola and E. Kerr, *Science*, 2004, **304**, 1648–1650.